Int. J. Multiphase Flow Vol. 9, No. 1, pp. 73–85, 1983
Printed in Great Britain.

0301-9322/83/010073-13$03.00/0
Pergamon/Elsevier

EFFECT OF FLOW-OBSTRUCTION GEOMETRY ON PRESSURE DROPS IN HORIZONTAL AIR–WATER FLOW

MARTHA SALCUDEAN
University of Ottawa, Ottawa, Ontario, Canada

DIONYSIUS C. GROENEVELD
Atomic Energy of Canada Limited, Chalk River, Ontario, Canada

and

LAURENCE LEUNG
University of Ottawa, Ottawa, Ontario, Canada

(*Received* 10 *November* 1981; *in revised form* 29 *June* 1982)

Abstract—Experiments were carried out to investigate the pressure drop due to flow obstructions in horizontal air–water flow. The axial pressure distribution along a 25.4 mm inside diameter tube, with and without flow obstructions was measured using multi-tube manometers. Various obstruction shapes and sizes were investigated. Pressure-loss coefficients and two-phase multipliers were derived for twelve different flow obstructions.

Estimates of the kinetic energy and momentum of the flow were also obtained from radial void distribution measurements. The pressure drop through the obstructions in two-phase flow was found to depend strongly on the kinetic energy and momentum of the liquid intercepted by the flow obstruction. Buoyancy-induced flow stratification caused a strongly non-symmetrical effect, and resulted in large pressure drops for flow obstructions located in the bottom part of the channel.

1. INTRODUCTION

The purpose of the present study is to investigate the pressure drop for horizontal two-phase flow through various flow obstruction shapes. The problem is relevant to many two-phase flow systems and can be encountered in the petroleum and nuclear plants. Examples of applications are partially closed valves in gas–liquid pipelines, and rod spacing devices in nuclear fuel assemblies. Flow obstructions increase the hydraulic resistance, hence more power is needed to maintain a given mass flow-rate in the system. In addition, obstructions can also have considerable influence on the heat transfer (Groeneveld & Yousef 1980).

Pressure drops through obstructions in two-phase flow are usually expressed by multiplying the single-phase pressure drop by a two-phase multiplier. The two-phase multiplier depends on several parameters, one of them being the relative velocity between the phases. The obstructions can induce significant mixing and change the phase and velocity distribution. Janssen (1966) studied the phase distribution across an orifice using high-speed photography and noted a change in the flow regime to a finely homogenized mixture downstream from the orifice with a velocity ratio likely to be unity. This suggests that the homogeneous pressure-drop model is the appropriate one to apply for the computation of pressure drop through such an orifice. Separated flow models were assumed by Lottes (1961) and Baroczy (1958), both of whom assumed an unchanged void-fraction across the obstruction. Experiments by Richardson (1958) mainly obtained for laminar flow, supported this assumption. Chisholm has developed a correlation for the pressure drop for the two-phase flow in pipes and through orifices and venturies, which introduced the shear forces between the phases (Chisholm 1967). Chisholm further developed the correlation to predict the pressure drop during two-phase flow through fittings (Chisholm & Sutherland 1969) and a simpler equation was presented by the same author (Chisholm 1971). The experimental results thus suggest that the effect of the obstruction on the change in phase and velocity distribution depends upon the obstructed area, obstruction shape, flow regimes, etc. For horizontal flow, the problem can become more complex if gravitational effects are significant.

In this paper, the influence of the degree of flow blockage and the shape of the flow obstructions on pressure drop was examined and two-phase multipliers were computed for the different obstructions. The effect of flow stratification on the two-phase multiplier was also investigated; the experimental results were explained in terms of momentum and kinetic energy intercepted by the flow obstructions.

2. EXPERIMENTAL METHOD

Figure 1 shows, schematically, the experimental test facility. The test section consists of a 25.4 mm I.D. 3-m long horizontal lucite tube, preceded by a honeycomb mixer and a 3-m calming length. A Meriam 33KB35 multi-tube manometer was used to measure the pressure gradient along the test section. Meriam oil with specific gravity of 2.95 was used as manometric fluid. The manometer is connected to the pressure taps and the reference pressure reservoir which, in turn, is connected to a pressure tap downstream from the obstruction. Toggle valves are installed between the columns and the pressure taps and also between the columns and the pressure reservoir. These valves could all be closed simultaneously, thus permitting the storage of the liquid columns of the manometer. A precise Bourdon-type pressure gauge is mounted on the pressure reservoir to measure the static pressure at the reference point. By-pass lines are provided to remove the air bubbles from inside the connecting lines which otherwise will affect the pressure readings. Further details of the experimental equipment and operating procedure may be found in Chun (1980).

Figure 2 illustrates the shapes of the flow obstructions. Six different shapes were in-

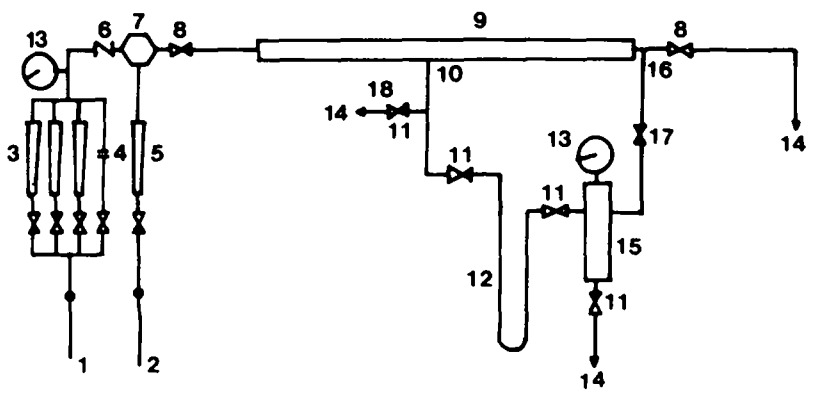

1	AIR SUPPLY	10	PRESSURE TAP
2	WATER SUPPLY	11	TOGGLE VALVE
3	ROTAMETER (air)	12	MANOMETER
4	ORIFICE PLATE (air)	13	PRESSURE GAGE
5	ROTAMETER (water)	14	TO DRAIN
6	CHECK VALVE	15	RESERVOIR
7	AIR-WATER MIXER	16	REF. TAP
8	THROTTLE VALVE	17	QUICK-CONNECTING VALVE
9	TEST SECTION	18	BY-PASSING LINE

Figure 1. Schematic diagram of the experimental loop.

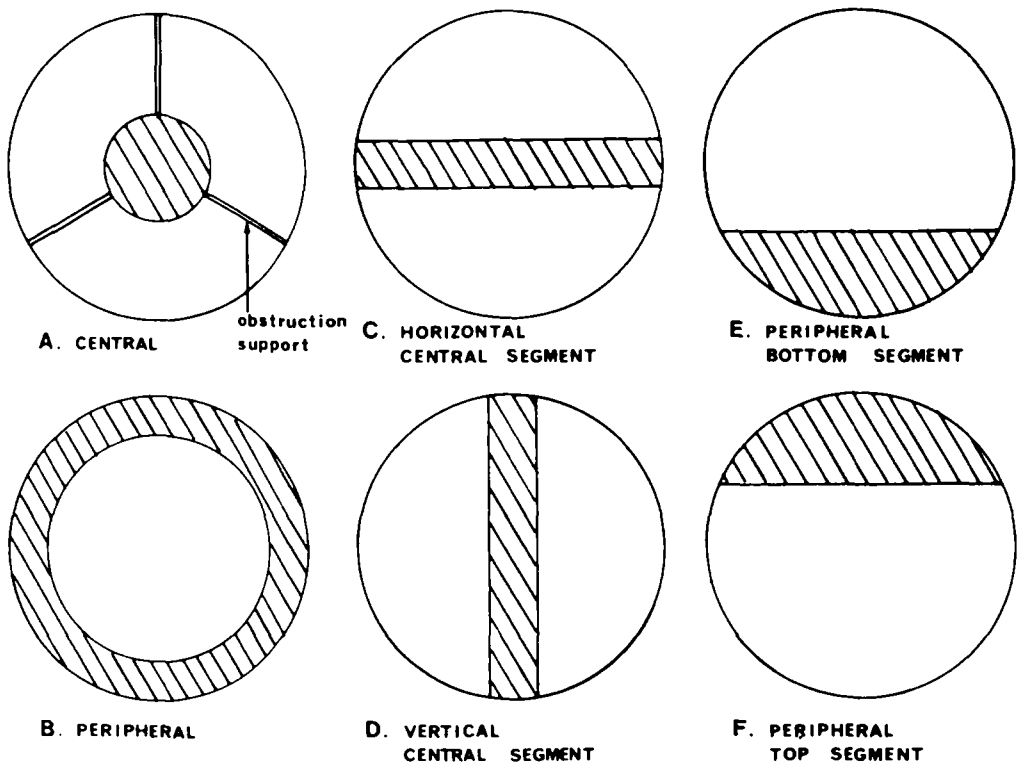

Figure 2. Shape and location of the obstruction in the channel.

vestigated for both the 25% and 40% flow blockage (the flow blockage is defined here as the percentage of the area of the channel cross-section occupied by the obstruction).

Measurements of flow obstruction pressure drop were obtained in single-phase flow and in two-phase flow (annular flow regime). The water superficial velocity was 0.59 m.s.$^{-1}$ and the air flow rate was varied up to 29 m.s^{-1} superficial velocity. The pressure at the obstruction varied between 163 and 385 kPa.

To understand the effect of the flow obstruction on the pressure drop, it is essential to know the phase distribution in the test section upstream from the flow obstruction. Phase distributions were obtained using a DISA miniature fibre-optic probe (Chun 1980, Salcudean *et al.* 1981). Basically a rotatable test section was used equipped with sliding optical probes. One-half of the test-section cross-section was divided in 95 sub-areas (the phase distribution was assumed to be symmetric with respect to the vertical axis). Measurements of void fraction in the centre of each sub-area were averaged over various time intervals (1, 10, 100, s). Figure 3 shows a void distribution map obtained for conditions of interest in this study (Salcudean *et al.* 1981).

3. RESULTS

3.1 *General*

Figures 4 and 5 illustrate the observed axial pressure distribution. Five separate regions were observed, both in single and two-phase flows. Regions I and V represent the undisturbed channel flow. Region II displays a stagnation effect of the flow obstruction, resulting in a levelling off of the pressure. Region III shows a rapid drop in pressure due to a pressure-energy conversion into increased kinetic energy and an increased turbulence level. Significant flashing may occur due to the corresponding drop in the saturation temperature for one-component two-phase flows. In region IV, some of the pressure is recovered as the velocity drops and the turbulence level decays. (The unrecovered pressure energy is dissipated). Figures 4 and 5 also

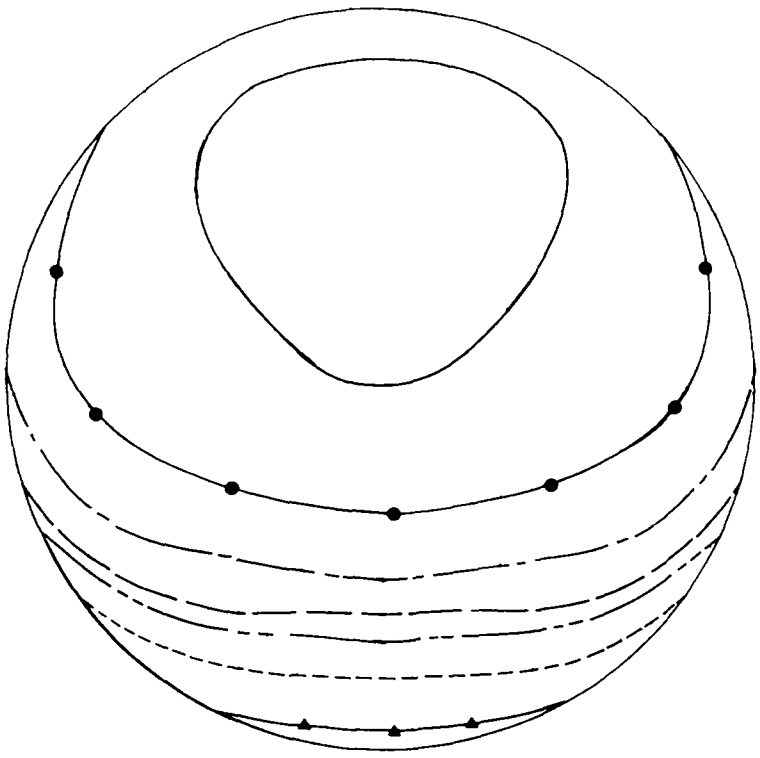

Figure 3. Void fraction distribution for non-obstructed horizontal flow.

show the obstruction pressure drop, defined usually as the increase in pressure drop due to the presence of a flow obstruction.

3.2 *Single-phase pressure drop*

The increase in single-phase pressure drop due to the presence of a flow obstruction may be expressed as:

$$\Delta p_{ob} = K_{ob}\frac{\rho_L V_0^2}{2} + f_{ob}\frac{t}{De_{ob}}\frac{\rho_L V_{ob}^2}{2} - f_0\frac{t}{De}\frac{\rho_L V_0^2}{2} \quad [1]$$

where Δp_{ob} is the pressure drop due to the obstruction, K_{ob} is the pressure loss coefficient for the obstruction, ρ_L is the density of the liquid, V_0 is the average velocity in the channel, f_{ob} is the friction factor of the obstruction, t is the thickness of the obstruction, De_{ob} is the equivalent hydraulic diameter of the obstruction, V_{ob} is the velocity of flow across the obstruction, f_0 is the friction factor of the channel, De is the equivalent hydraulic diameter of the channel.

The first term on the r.h.s. of [1] represents the obstruction pressure drop, the second term the skin friction pressure drop over the obstruction length and the third term the pressure drop

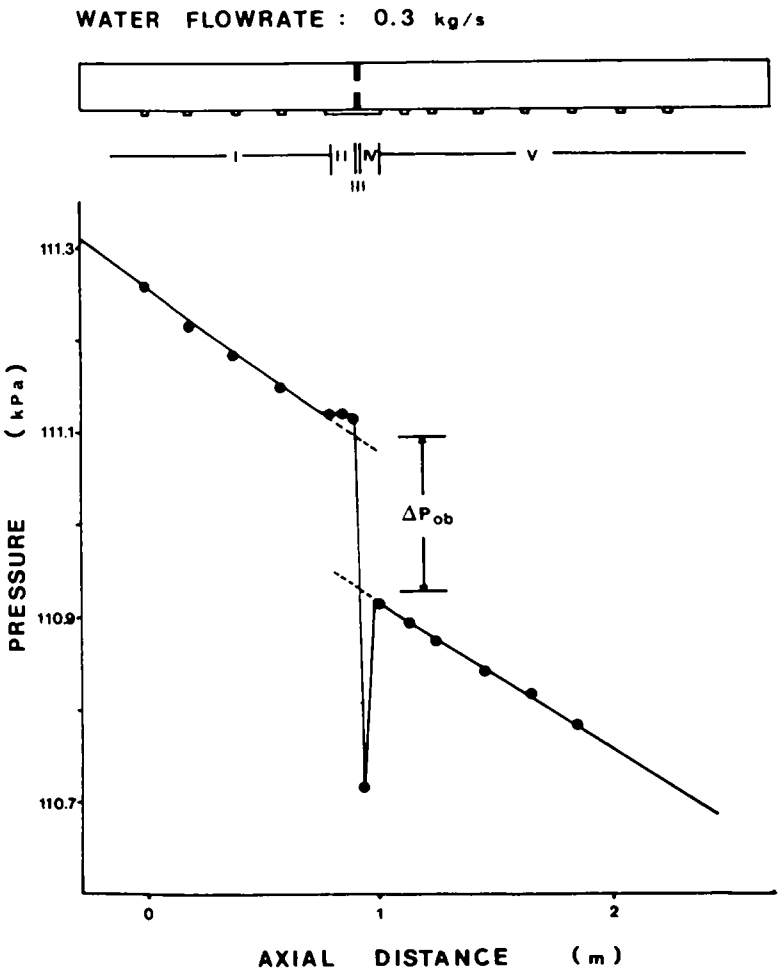

Figure 4. Pressure profile for single-phase (water) flow.

in the channel without obstruction over the obstruction length. The friction factors f_0 and f_{ob} are evaluated from Colebrook or equivalent correlations. As "t", the obstruction thickness, was small for this investigation, the pressure drop may be approximated by

$$\Delta P_{ob} = K_{ob} \frac{\rho_L V_0^2}{2} \qquad [2]$$

where K_{ob} is an overall pressure-loss coefficient.

The pressure-drop coefficients for the obstructions illustrated in figure 2 are presented in table 1. This table also shows the momentum and the kinetic-energy ratios of the obstructions defined as follows:

$$r_{mom} = \left(\int^{A_{ob}} V^2 \, dA\right) \Big/ \left(\int^{A_0} V^2 \, dA\right) \qquad [3]$$

and

$$r_{k.e.} = \left(\int^{A_{ob}} V^3 \, dA\right) \Big/ \left(\int^{A_0} V^3 \, dA\right) \qquad [4]$$

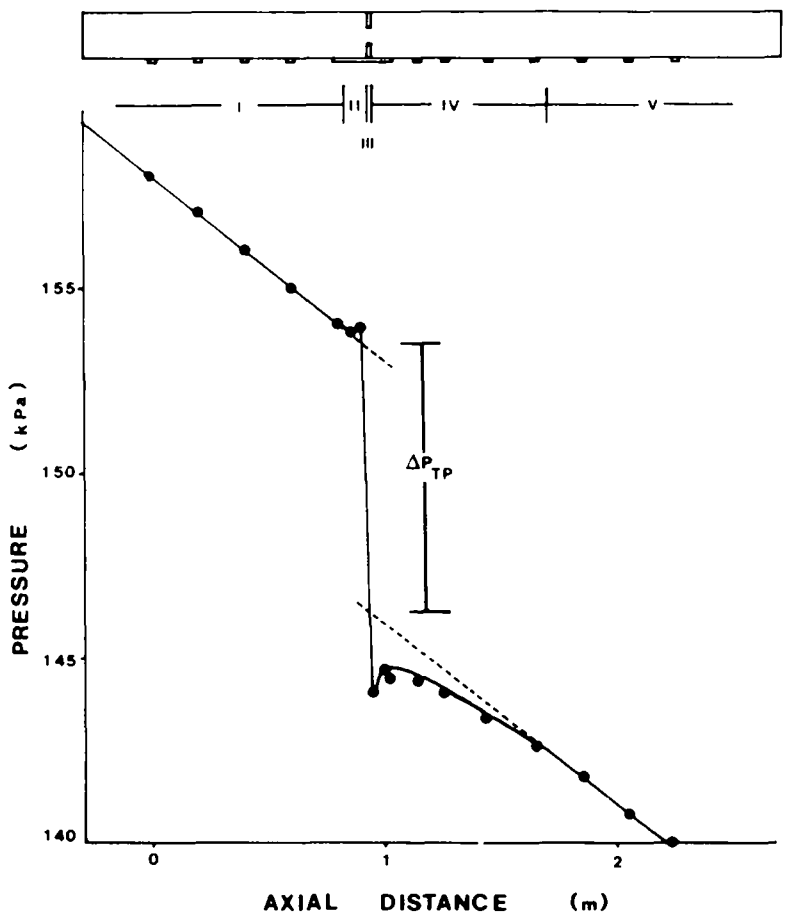

Figure 5. Pressure profile for two-phase flow.

Table 1. Pressure loss coefficient K, momentum ratio, r_{mom}, and kinetic energy ratios, r_{ke}, for single-phase flow

Obstruction Shape (Fig. 3)		Flow Blockage - 25%			Flow Blockage - 40%		
		K	r_{mom}	r_{ke}	K	r_{mom}	r_{ke}
Peripheral	B	0.27	0.10	0.06	1.37	0.36	0.19
Central	A	0.81	0.22	0.20	2.40	0.55	0.50
Horizontal Central Segment	C	0.86	0.16	0.16	2.58	0.29	0.25
Vertical Central Segment	D	0.97	0.16	0.16	2.67	0.29	0.25
Peripheral Bottom Segment	E	0.59	0.145	0.11	1.98	0.247	0.20
Peripheral Top Segment	F	0.58	0.145	0.11	1.97	0.247	0.20

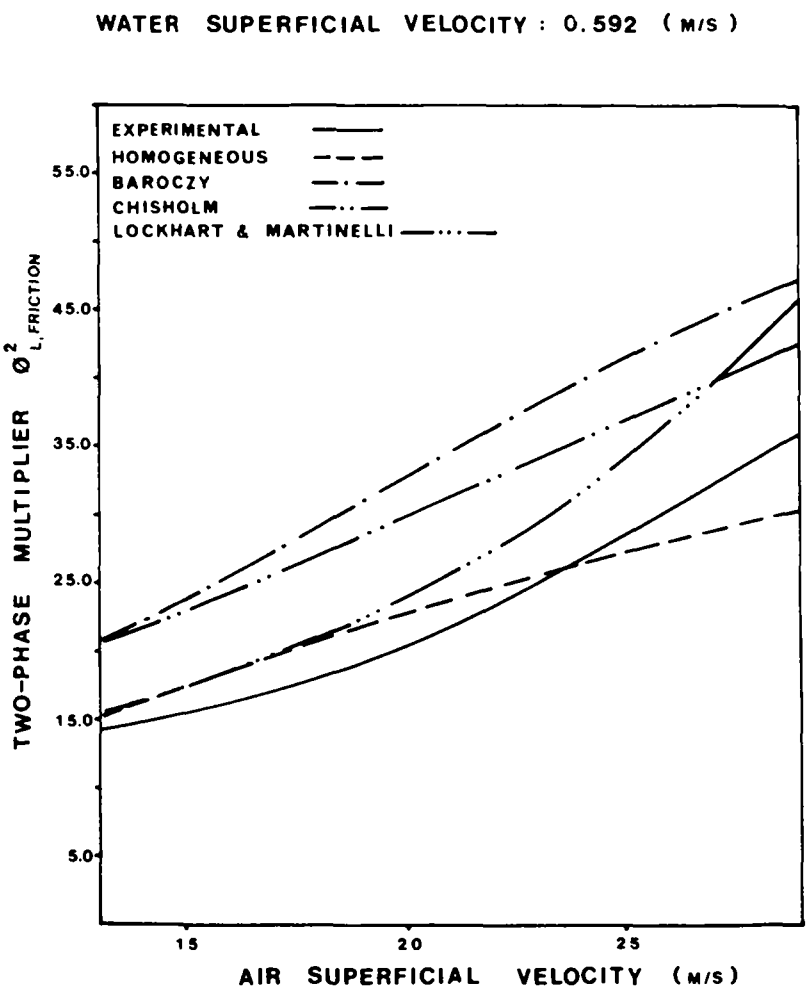

Figure 6. Two-phase frictional pressure drop multiplier comparison with the homogeneous two-phase multiplier.

where r_{mom} is the momentum ratio, $r_{k.e.}$ is the kinetic energy ratio, A_{ob} is the obstruction area, A_0 is the channel area, V is the velocity of the flow.

The momentum ratio, r_{mom}, was computed by integrating the momentum (based on the local velocity in the undisturbed fluid) over the obstructed area and over the channel area.

The kinetic energy ratio, $r_{k.e.}$, was computed by integrating the kinetic energy (based on the local velocity in the undisturbed fluid) over the obstructed area and over the channel area.

A turbulent profile with power law variation was assumed. As expected, for all obstruction shapes, the 40% obstruction produced a larger pressure drop than the 25% obstruction.

The largest pressure drops were produced by the central segments and the central obstruction for both 25% and 40% ratios.† This is in agreement with the momentum and the kinetic energy ratios and is probably due to the interception of the high velocity flow.

One can see that a large momentum and kinetic energy ratio is associated generally with larger pressure-loss coefficients. The lowest pressure-loss coefficients are due to the peripheral obstructions, as they obstruct the lower velocity region near the wall. The vertical and

†The central obstructions including the supports block a total of 25% and respectively 40% of the channel area. Therefore, as compared with an ideal case of central obstruction, the drag is decreased due to a smaller blockage in the higher velocity central region. On the other hand, a slight increase of the drag is expected due to the effect of the supports. The calculations were carried out for the ideal geometry of a central disk.

horizontal segments produce larger pressure drops than the peripheral segments for both 25% and 40% obstructions, since they intercept the higher velocity fluid.

It is likely that the obstruction shape influences also the turbulence generation and the Re-attachment point. This influence cannot be quantified by the present kinetic energy and momentum calculations.

The differences in measured pressure-loss coefficients between the obstructions C and D (same obstruction, rotated 90°) and between E and F (same obstruction, rotated 180°), are due to experimental errors.

3.3 *Two-phase flow pressure drop*

3.3.1 *Two-phase multiplier before the obstruction.* Figure 6 illustrates the two-phase multiplier as a function of the air superficial velocity determined from the measurements using the relation:

$$\phi_L^2 = \frac{\left(\frac{dP}{dz}\right)_{TP}}{\left(\frac{dP}{dz}\right)_L} \quad [5]$$

where ϕ_L^2 is the two-phase multiplier, $(dP/dz)_{TP}$ is the two-phase frictional pressure drop, $(dP/dz)_L$ is the single-phase frictional pressure drop which is evaluated from single-phase experiments having a liquid velocity equal to the superficial liquid velocity. In the same graph, the Lockhart–Martinelli (1949), Baroczy (1965), Chisholm (1969) and the homogeneous† two-phase multiplier (Collier 1972) are presented for comparison.

3.3.2 *Pressure drop due to obstruction.* Figures 7 and 8 illustrate the dimensionless pressure drop caused by the different obstructions after the pressure recovery occurred (see figure 4). The dimensionless pressure drop is defined here as:

$$\Delta P^+_{TP,ob} = \frac{\Delta P_{TP,ob}}{\rho_L V_0^2/2} \quad [6]$$

where V_0 is the superficial liquid velocity and $\Delta P_{TP,ob}$ is the obstruction pressure drop as defined in figure 5. Note that this representation serves to compare all two-phase flow obstruction pressure drops with a single-phase pressure drop, at the same superficial liquid velocity.

Figures 7 and 8 show that the lowest pressure drop is given by the top segment while the greatest is given by the bottom segment. This is clearly an effect of flow separation due to buoyancy forces. The bottom segment intercepts more of the liquid phase, while the top segment intercepts more of the gaseous phase. For the same reason, the vertical segment is associated with larger pressure drops than is the horizontal segment. The peripheral obstruction, which was associated with the lowest pressure drop in single-phase flow, produces a relatively larger pressure drop as it intercepts the liquid annulus.

In order to explain the trends in a more quantitative manner, an integration of the momentum and the kinetic energy of the obstructed two-phase flow was carried out. The calculations were based on the following assumptions:

†The homogeneous two-phase multiplier is defined as

$$\phi_L^2 = \left(1 + x\frac{v_{LG}}{v_L}\right)\left(1 + x\frac{\mu_{LG}}{\mu_G}\right)^{-1/4} \Big/ (1-x)^{1.75}$$

where x is the quality, v is the specific volume, μ is the viscosity.

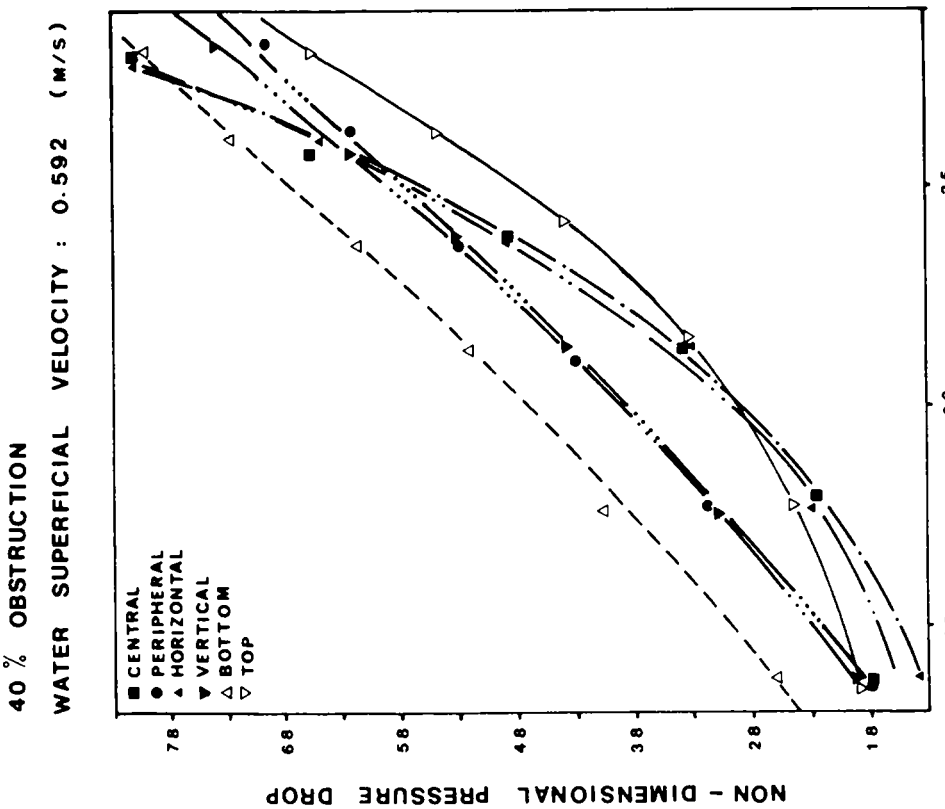

Figure 8. Non-dimensional obstruction pressure drop for 40% obstructions.

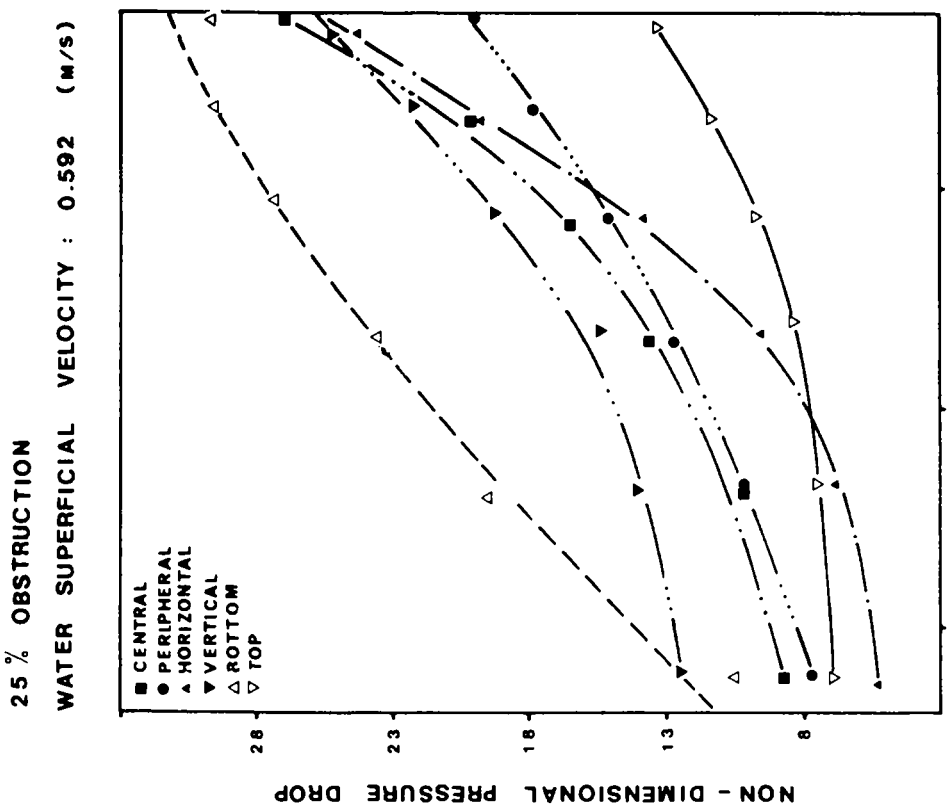

Figure 7. Non-dimensional obstruction pressure drop for 25% obstructions.

—a turbulent profile with power-law variation was assumed in the thin liquid annulus surrounding the channel surface;

—uniform velocity was assumed in the bulk of the liquid and gas flows, equal to the average velocity of each phase;

—along the channel axis (high void region), the entrained water was assumed to flow at the same velocity as the gas flow, an assumption which leads to an overestimation of the momentum and the kinetic energy ratio.

These assumptions are crude approximations, necessary because of the lack of knowledge of velocity distributions. Also, the phase distribution plays a considerably more important role in determining the momentum value than does the velocity distribution. This is due to the large density difference between the phases.

Figure 3 illustrates the void distribution in the channel for a gas weight fraction of 4.55%. The void measurements were carried out with optical probes (Salcudean *et al.* 1981). One can notice from table 2 that the trend observed experimentally coincides with the trend of the computed values. This table illustrates the values of the momentum and kinetic energy ratios. One can notice that the experimentally found pressure drop variation trends are generally in agreement with the computed momentum and kinetic energy ratio variation. The large momentum and kinetic energy ratios are associated with larger pressure drops.

Figures 9 and 10 illustrate the variation of the obstruction two-phase multiplier as a function of the superficial air velocity. The two-phase multiplier for flow obstructions is defined as:

$$\phi_{L,\mathrm{ob}}^2 = \frac{\Delta P_{TP,\mathrm{ob}}}{K_{\mathrm{ob}} \dfrac{\rho_L V_0^2}{2}} \qquad [7]$$

where K_{ob} was evaluated as described previously. Note the similarity of [7] with [6] for the dimensionless obstruction pressure drop. One can deduce that the two-phase multiplier depends strongly on the obstruction shape and location. The largest values are produced by peripheral obstructions and are due to the interception of the liquid phase. For one-phase flow, the peripheral obstruction intercepts the lowest-velocity fluid and, thus, the pressure loss coefficient is considerably lower than for the other obstruction shapes. For two-phase flow, the peripheral obstruction intercepts the liquid phase and this difference accounts for the large two-phase flow

Table 2. Momentum ratio, r_{mom}, and kinetic energy ratio, $r_{k.e}$, for two-phase flow

Obstruction Shape (Fig. 3)		Flow Blockage - 25%		Flow Blockage - 40%	
		r_{mom}	$r_{k.e.}$	r_{mom}	$r_{k.e.}$
Peripheral	B	0.084	0.05	0.109	0.07
Central	A	0.117	0.27	0.252	0.57
Horizontal Central Segment	C	0.042	0.06	0.083	0.13
Vertical Central Segment	D	0.053	0.07	0.097	0.14
Peripheral Bottom Segment	E	0.086	0.07	0.11	0.09
Peripheral Top Segment	F	0.03	0.02	0.041	0.03

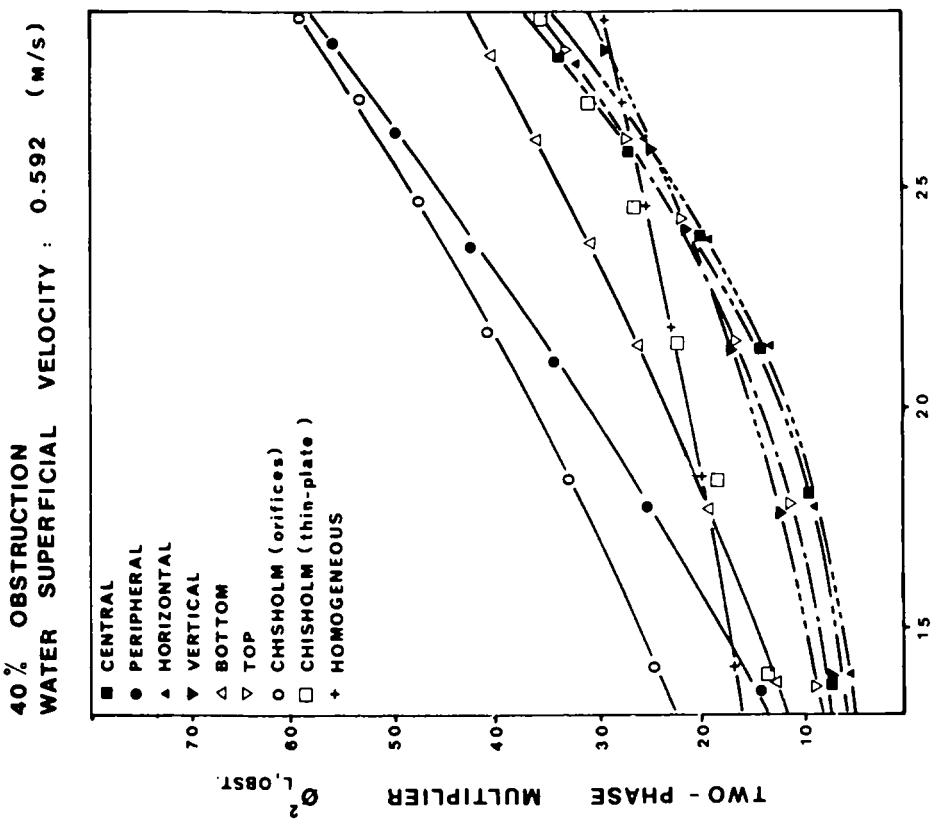

Figure 10. Two-phase obstruction pressure drop multiplier for 40% obstructions.

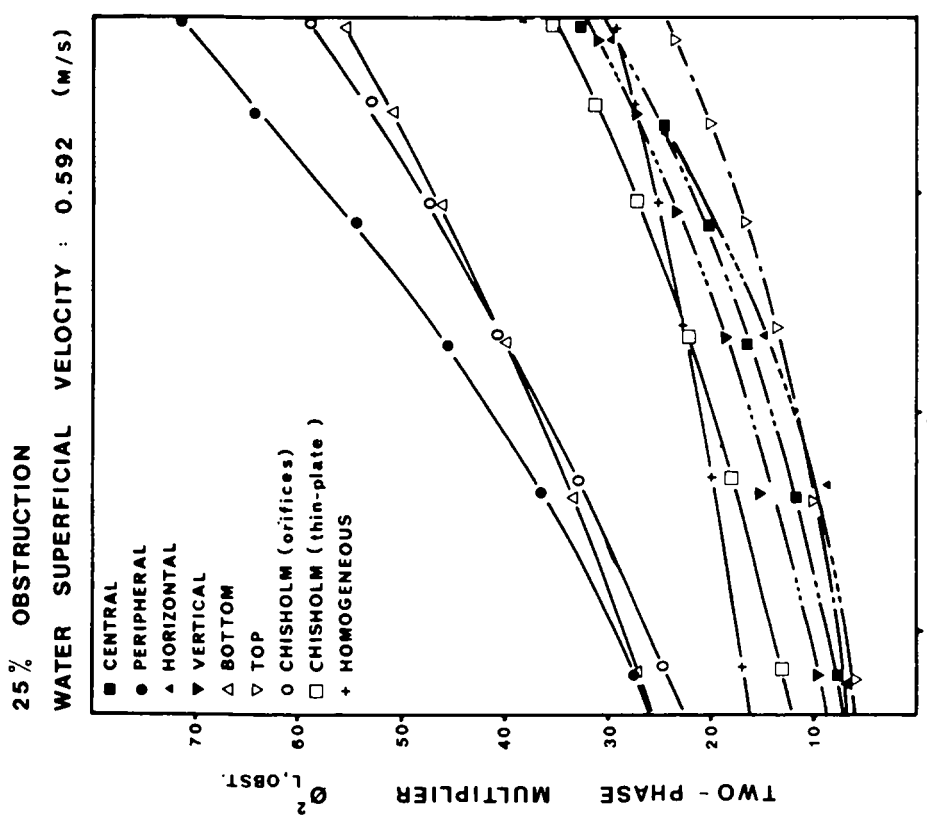

Figure 9. Two-phase obstruction pressure drop multiplier for 25% obstructions.

multiplier. The second largest two-phase multiplier is produced by the bottom segment, while the small values were recorded for the top segments. The different effect is a result of the flow stratification.

The low two-phase multiplier for the central obstruction is due to its intercepting the gaseous phase. In figures 9 and 10, the homogeneous two-phase multiplier and the Chisholm correlation† for orifices and thin plates are illustrated for comparison.

SUMMARY

The pressure drops through obstructions in horizontal two-phase flow were investigated. Measurements were carried out for two different flow blockages and six obstruction shapes.

Initially, the pressure-loss coefficient was determined for single-phase flow. The highest pressure drops were observed for central and central segment obstructions and the lowest for peripheral obstructions. This was compared with calculated momentum and kinetic energy ratios. Larger values of momentum and kinetic energy ratios (fluid with higher momentum and kinetic energy ratios is intercepted by the obstructions) were associated with larger pressure drops.

The two-phase flow pressure drops through the obstructions proved to be largely dependent upon obstruction location at a given cross-section.

The obstructions intercepting more of the liquid phase produced considerably larger pressure drops than those located in the gaseous phase; the top segment produced the lowest pressure drop, while the bottom segment produced the highest.

The measured pressure drops showed generally an increase with the increase of the calculated momentum and kinetic energy ratios.

The obstruction two-phase multipliers were highest for obstructions intercepting mainly the liquid phase.

Acknowledgements—The authors wish to acknowledge the assistance of Mr. J. H. Chun, who constructed the experimental facility loop. Financial support was provided by Atomic Energy of Canada Ltd.

REFERENCES

BAROCZY, C. J. 1958 *A Systematic Correlation for Two-phase Two-component Flow.* ANL-5949.

BAROCZY, C. J. 1965 A systematic correlation for two-phase pressure drop. A.I.Ch.E. reprint No. 37, Paper presented at 8th Nat. Heat Transfer Conf., Los Angeles.

CHISHOLM, D. 1967 Flow of incompressible two-phase mixtures through sharp-edged orifices. *J. Mech. Engng Sci.* **9**, 72–78.

CHISHOLM, 1967 Pressure gradients during the flow of incompressible two-phase mixtures through pipes, Venturi and orifice plates. *Br. Chem. Engng* **12**, 454–457.

CHISHOLM, D. & SUTHERLAND, L. A. 1969 Prediction of pressure gradients in pipeline systems during two-phase flow. Paper 4 presented at Symp. on Fluid Mechanics and Measurements in Two-phase Flow Systems, Leeds, 24–25.

CHISHOLM, D. 1971 Prediction of pressure drop at pipe fittings during two-phase flow. Proc. 13th *Int. Inst. of Refrig. Congress*, Washington, D.C. 29 Aug.–3 Sept., **2**, 781–789.

CHUN, J. H. 1980 Flow stratification in two-phase flow in horizontal channels. M.A.Sc. Thesis, University of Ottawa.

COLLIER, J. G. 1972 *Convective Boiling and Condensation.* McGraw-Hill, New York.

GROENEVELD, D. C. & YOUSEF, W. W. 1980 Spacing devices for nuclear fuel bundles: a survey of their effect on CHF, post-CHF heat transfer and pressure drop. Paper presented at ANS/ASME Topical Meeting on Nuclear Reactor Thermohydraulics, Saratoga, New York.

†The viscosity correction was not included by Chisholm in his correlation (Chisholm 1971).

JANSSEN, E. 1966 Two-phase pressure loss across abrupt contractions and expansions, steam–water at 600 to 1400 psia. *Proc. 3rd Int. Heat Transfer Conf., Chicago*, 13–23.

LOCKHART, R. W. & MARTINELLI, R. C. 1949 Proposed correlation of data for isothermal two-phase two-component flow in pipes. *Chem. Engng Prog.* **45**, 39–48.

LOTTES, P. A. 1961 Expansion losses in two-phase flow. *Nucl. Sci. Engng* **9**, 26–31.

RICHARDSON, B. L. 1958 Some problems in horizontal two-phase two-component flow. ANL-5949.

SALCUDEAN, M., CHUN, J. H., & GROENEVELD, D. C. 1983 Effect of flow obstruction on void distribution in horizontal air–water flow. *Int. J. Multiphase Flow* **9**, 91–96.